

SITE CHARACTERIZATION REPORT

SAPK: Appenzell (AI) - Kantonsschule

Clotaire Michel, Paolo Bergamo, Manuel Hobiger, Donat Fäh



Last Modification: 20th January, 2017

Schweizerischer Erdbebendienst (SED)
Service Sismologique Suisse
Servizio Sismico Svizzero
Servizi da Terratrembels Svizzer

ETH Zurich
Sonneggstrasse 5
8092 Zurich
Schweiz
clotaire@sed.ethz.ch

Contents

Contents	3
1 Introduction	5
2 Geological setting	6
3 Site characterization using passive measurements	7
3.1 Measurements and data set	7
3.2 Single station measurements results	9
3.2.1 H/V curves	9
3.2.2 Polarization analysis	13
3.3 3-component high-resolution FK	14
3.4 Wavedec	15
3.5 Interpretation	16
3.6 Data inversion	17
3.6.1 Misfit function	17
3.6.2 Parametrization of the model space	17
3.6.3 Results	17
4 Interpretation of the velocity profiles	20
4.1 Velocity profiles	20
4.2 Quarter-wavelength representation	21
4.3 SH transfer function	21
5 Conclusions	24
References	24

Summary

The new station SAPK was installed in the town of Appenzell (AI) and the installation site has been characterized. We performed passive seismic array measurements that successfully allowed to retrieve the 1D velocity profile at the station site. The soft sediment cover (moraine) is about 17 m thick with a low shear wave velocity over the 5 first meters and of about 500 m/s below. The rock located underneath (Lower Freshwater Molasse) has a shear wave velocity of about 1000 m/s. The thickness of the cover is variable below the town.

$V_{s,30}$ is 509 m/s and the site corresponds to ground type E in the Eurocode 8 (CEN, 2004) and in the SIA261 (SIA, 2014). The theoretical 1D SH transfer function computed from the inverted profiles shows an amplification of a factor of 2 to 3 at the resonance frequencies of the site at 4 and 7 Hz.

1 Introduction

In the framework of the second phase of the Swiss Strong Motion Network (SSMNet) renewal project, a new installation in the secondary school in Appenzell (AI) was decided. It is located in hilly area of the Swiss foreland (see Fig. 1). The new station went operational on 10 December 2015.



Figure 1: Array measurement and station SAPK (on the left, close to a tree).

2 Geological setting

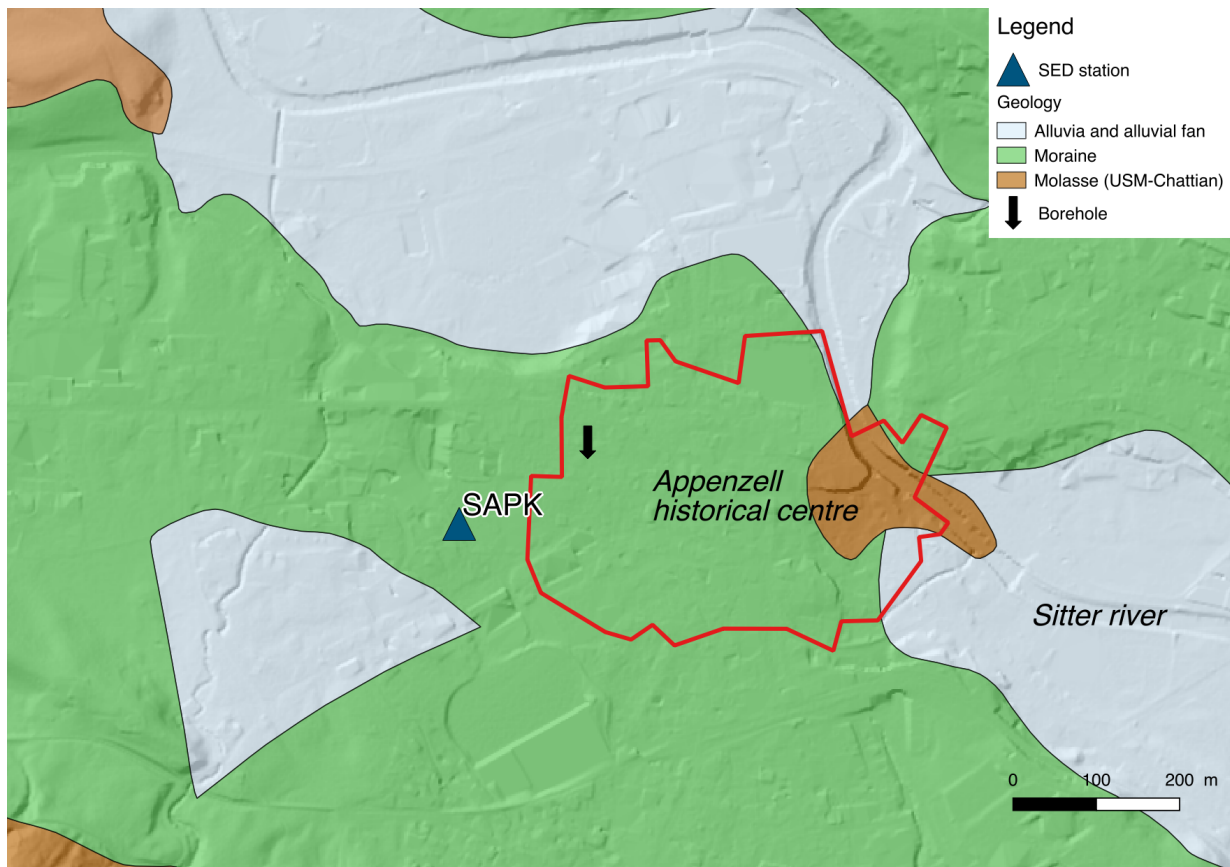


Figure 2: Geological map of the town of Appenzell including the location of the SAPK station and the available borehole (data: © 2016 swisstopo JD100042).

The site SAPK is located in the Swiss foreland, close to the alpine region. At the station site (Fig. 2), one finds moraine from the latest glaciation on top of the Lower Freshwater Molasse (USM) of Chattian age (Oligocene, Tertiary). The Molasse basin is about 5 km deep at that site. Although many boreholes appear on the geoportal of the Canton, it seems that few have actually been carried out, according to the canton. The only available borehole we could access is located Kronengarten 6 (Parzelle Nr. 102580) and shows 26 m of moraine on the Molasse rock made of sandstone and marls. No aquifer is present in this area. These conditions are representative of a large part of the city centre of Appenzell, though the thickness of the moraine varies. The molasse rock outcrops in the eastern part of the historical city centre.

3 Site characterization using passive measurements

3.1 Measurements and data set

We investigated the local underground structure by passive seismic array measurements, which took place on October 7th, 2016. The layout of the seismic arrays is shown in Fig. 3. Two configurations were used.

The parameters of both arrays are given in Table 1. For these measurements 12 Nanometrics Centaur dataloggers named NR42 to NR49 and NR52 to NR55 and 14 Lennartz 3C 5 s seismometers were available. Unfortunately, station NR49 was wrongly configured and the data are tagged with name NR52 (the conversion for this station had to be performed separately). Each datalogger can record on 2 ports A (channels EH1, EH2, EH3 for Z, N, E directions) and B (channels EH4, EH5, EH6 for Z, N, E directions). Time synchronization is ensured by GPS. The sensors were placed on metal tripods, in a 10 cm deep hole, when possible, for better coupling with the ground.

The sensor coordinates were measured using a differential GPS device (Leica Viva GS10), including only a rover station and using the Real Time Kinematic technique provided by Swisstopo. It allows an absolute positioning with an accuracy better than 5 cm on the Swissgrid.

Table 1: List of the seismic array measurements in Appenzell.

Array name	Number of sensors	Minimum interstation distance [m]	Aperture [m]	Recording time [min]
APK1	14	10	120	148
APK2	14	10	280	136

The largest time windows were extracted, for which all the sensors of the array were correctly placed and the GPS synchronization was ensured. A strong disturbance at 4 Hz in the vertical component can be noticed during the first configuration APK1 (source N of the array). Since it can be seen also on the E component of station APK305, this station was possibly not correctly leveled or had been touched (it was located on a parking place). A lot of undamped peaks can be seen, especially between 6 and 8 Hz. Station APK405, located along a main road, shows a very high noise and could be excluded, though it was kept in the following. Station APK401 also shows an elevated noise level, but not as much problematic. These disturbances affect the H/V analysis in section 3.2.1. Orientations of the sensors were checked by maximizing the correlation with the central station at low frequencies (Poggi et al., 2012b). Corrections lower than 9° were observed, except for station APK302 that deviates by 33° .

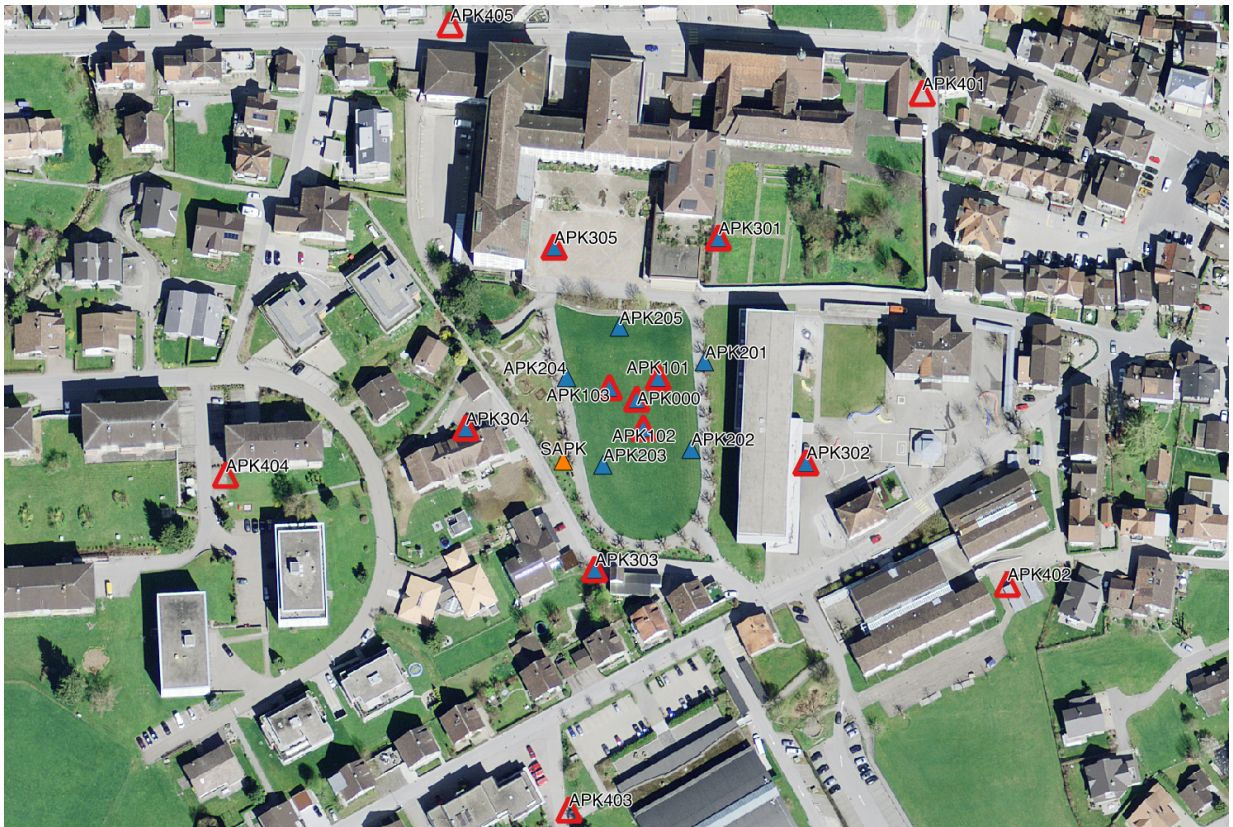


Figure 3: Layout of the array measurements at site SAPK; Dataset APK1 is depicted with blue triangles, APK2 in red.

3.2 Single station measurements results

3.2.1 H/V curves

This paragraph describes the results from all single station recordings available in the Appenzell town. A zoom of the available points is presented in Fig. 4. The interpretation of the H/V curves is made difficult by the numerous harmonic peaks of anthropogenic origin polluting the signal. The test stations XAPZ1 and XAPZ2, installed during one week in the school building help the interpretation (Fig. 5). They show that there is no peak in the H/V curves at low frequency: the apparent bump in Fig. 6 is therefore an artifact. They both show a relatively clear peak at about 4 Hz. The high frequencies are more difficult to interpret due to the numerous harmonic peaks. The first dataset APK1 is affected by an anthropogenic signal at 4.18 Hz as testified by the multitaper method (Prieto et al., 2009; Baumann et al., 2013), which is not the case of dataset APK2 (Fig. 6). Around this frequency, only APK2 should therefore be interpreted. The signal above 5 Hz in both cases is also much disturbed and difficult to interpret. However, the curves have been carefully picked accounting for all available information. It is possible to see on all curves of the APK2 dataset the 4 Hz peak. Slight variations are noticed between 3.5 and 4.5 Hz. The northern part of the study-area shows the lower frequencies, while the centre of the array has slightly higher values. Moreover, a second peak at 7.6 Hz, exaggerated by several harmonic disturbances is also seen in the central part of the array thanks to the multitaper method only (first ring and points 201 and 203; 204 and 205 are unclear and other points do not show this peak). Some other points show a peak at higher frequency (about 10 Hz).

The single stations recordings from the whole town have been repicked though they present the same issues of disturbances and the results should be taken with care (Fig. 7).

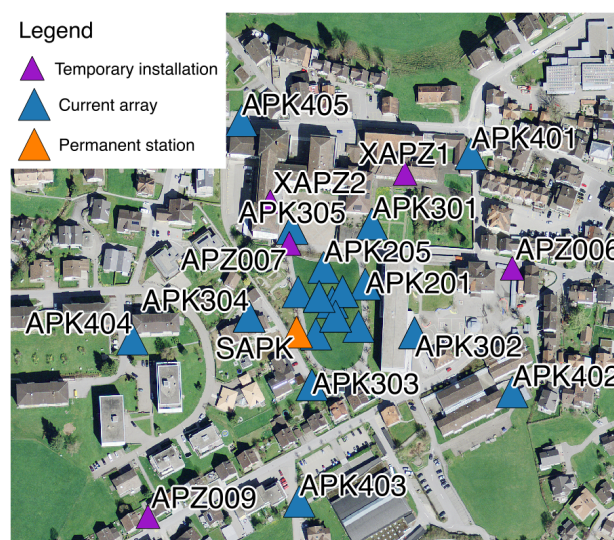


Figure 4: Available recordings in the area.

Moreover, all the methods to compute H/V ratios are compared at point APK000 in Fig. 8, in which the classical methods were divided by $\sqrt{2}$ to correct for the Love wave contribution (Fäh et al., 2001). The classical and TFA methods match well. The WaveDec method (see section 3.4) shows a change in the sign of the ellipticity at 7.6 Hz creating the peak that is also seen in the H/V curves but no peak at 4 Hz. The 3C FK analysis (Capon method) does not match the H/V analysis (see section 3.3).

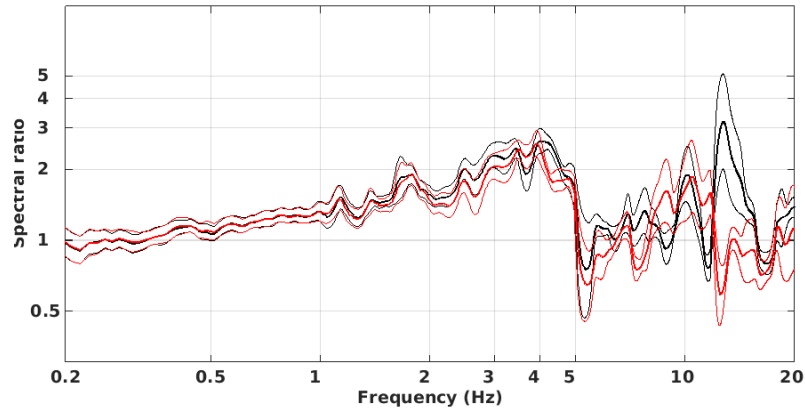


Figure 5: H/V ratios of temporary stations XAPZ1 (black) and XAPZ2 (red) located in the school building close to station SAPK (see map in Fig. 4).

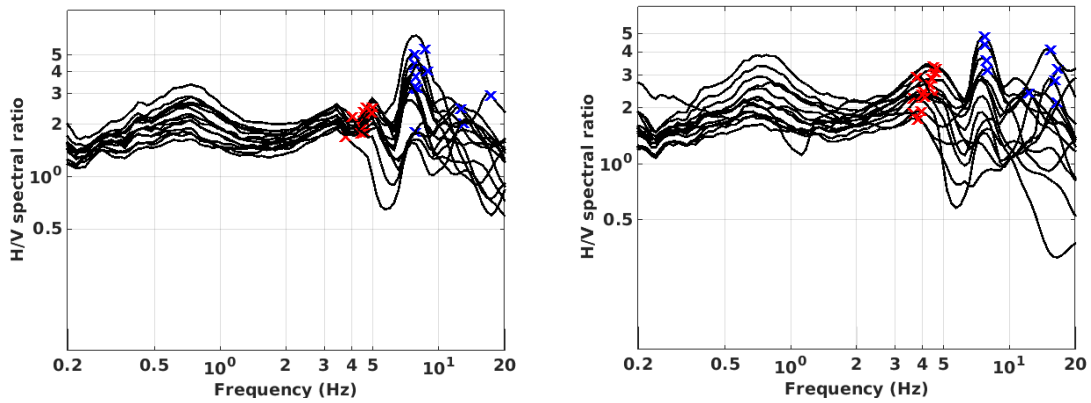


Figure 6: Comparison of H/V spectral ratios (time-frequency analysis code Poggi et al., 2012b) between the different points of the arrays (left: APK1, right: APK2). Note the effect of the vertical disturbance at 4.18 Hz during APK1.

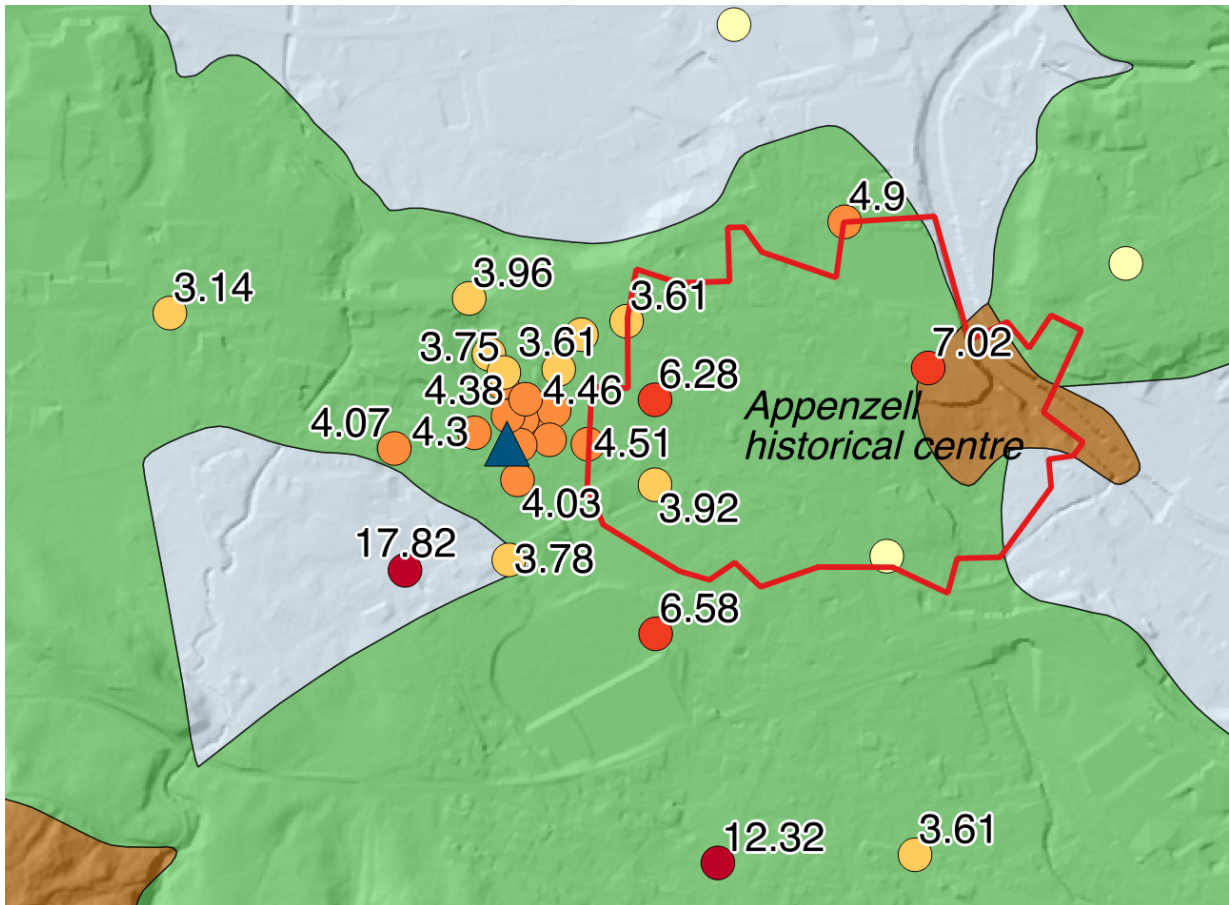


Figure 7: Maps of the identified peaks in the H/V ratios (frequency values in Hz) superimposed on the simplified geological map of the area (see Fig. 2 for the legend). The blue triangle is the SAPK station.

The fundamental peak at the SAPK station is therefore at 4.5 Hz, with a peak amplitude around 2.6.

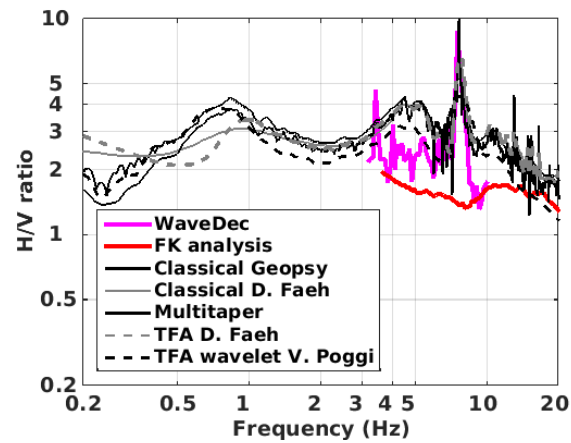


Figure 8: H/V spectral ratios for point APK000 using the different codes. Classical methods were divided by $\sqrt{2}$.

3.2.2 Polarization analysis

Polarization analysis on the array data was performed to check for 2D resonance using the method of Burjánek et al. (2010). The wavefield is slightly flatter at the fundamental frequency but no particular polarization could be noticed across the array (Fig. 9). We assume therefore that there is no 2D resonance of the valley at this site.

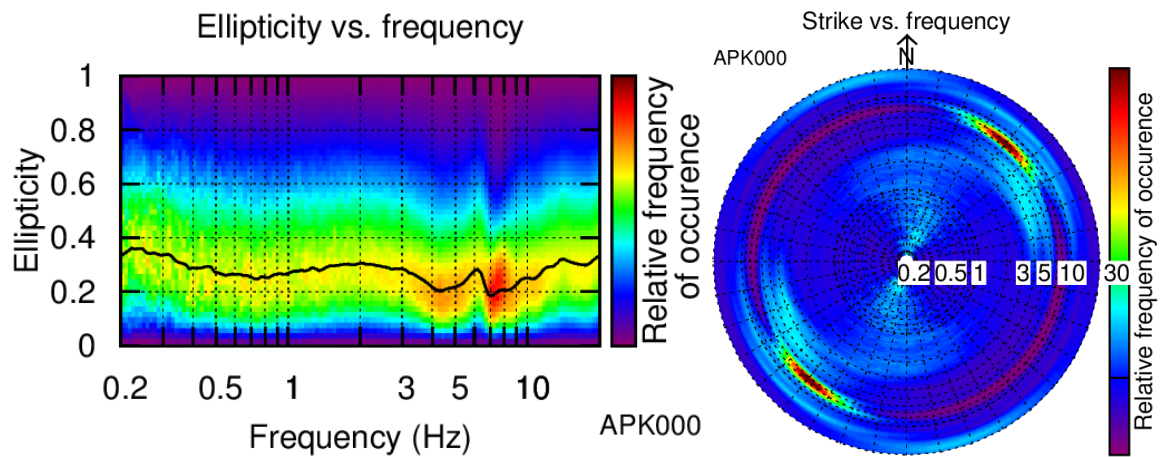


Figure 9: Polarization analysis at point APK000. Left: Ellipticity (A trough in the ellipticity corresponds to polarized motion). Right: Strike of the polarization.

3.3 3-component high-resolution FK

The results of the 3-component high-resolution FK analysis (Poggi and Fäh, 2010) for the merged results of both configurations are shown in Fig. 10. The fundamental modes of Rayleigh and Love waves are relatively clearly determined from this analysis between 3 and 3.5 Hz and 12 and 10.5 Hz, respectively. The first higher mode of Love waves is picked with some imagination from the transverse component.

The ellipticity curve determined with the 3-component HRFK analysis is described in the H/V analysis.

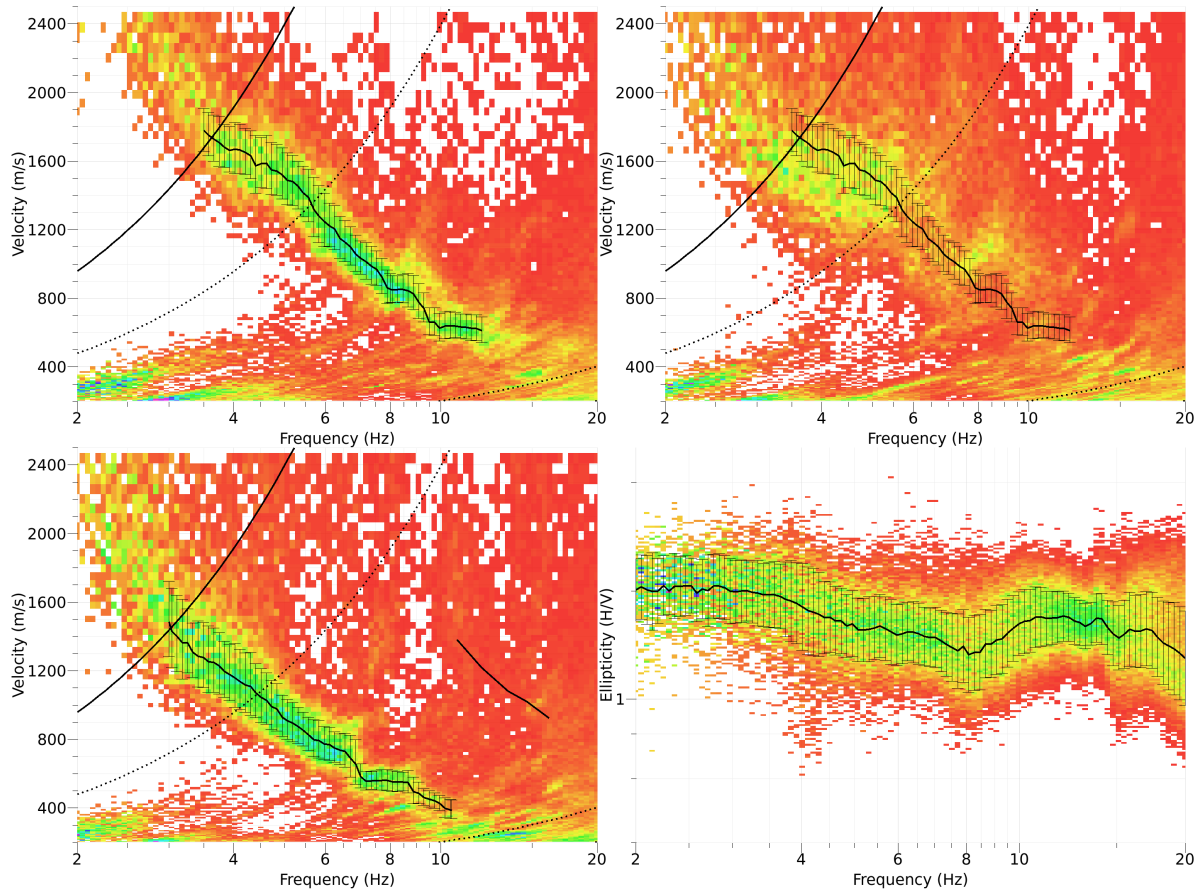


Figure 10: Dispersion curves obtained from the 3C HRFK analyses. From left to right and top to bottom: Vertical and radial dispersion, transverse dispersion and ellipticity (radial over vertical).

3.4 Wavedec

WaveDec (Maranò et al., 2012) has also been used to process the array data APK2. This technique estimates the properties of multiple waves simultaneously with a maximum likelihood approach in the time domain. It was applied assuming the presence of 3 waves and for a gamma parameter of 0.2, which causes less penalty on complexity and may result in a larger number of disturbances in the dispersion plot.

The fundamental Love and Rayleigh waves dispersion curves could be picked (Fig. 11) and are compared to the other analyses in section 3.5. The ellipticity of Rayleigh waves (Fig. 12) is compared with other proxys for the ellipticity curve in Fig. 8.

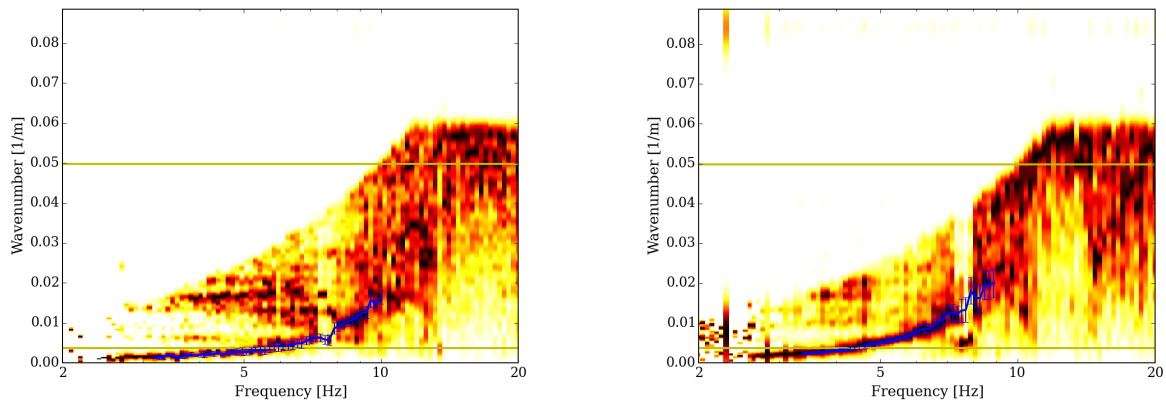


Figure 11: Rayleigh and Love wave dispersion curves obtained with the WaveDec technique (Maranò et al., 2012). The yellow lines indicate the theoretical array resolution limits.

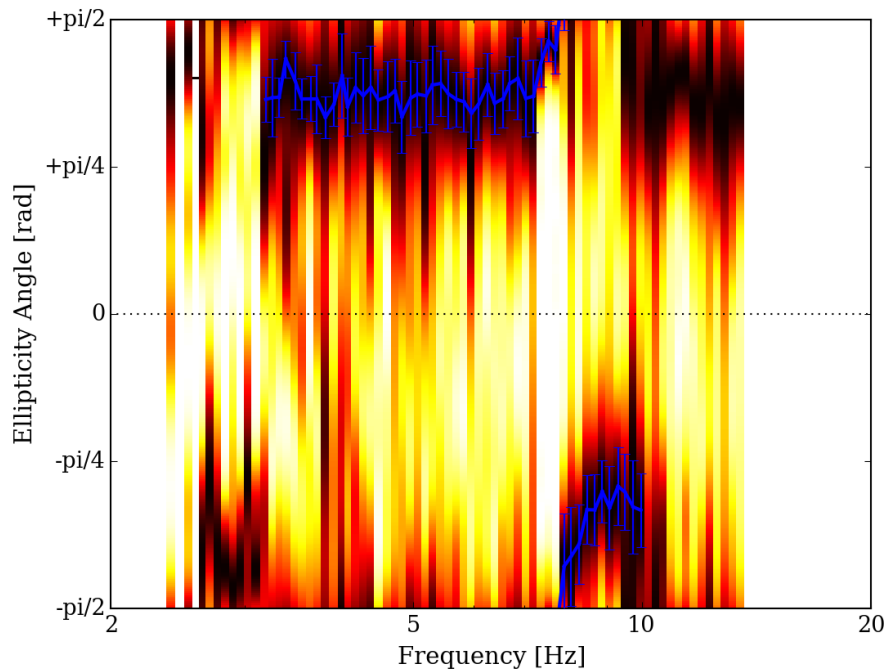


Figure 12: Rayleigh ellipticity curve obtained with the WaveDec technique (Maranò et al., 2012).

3.5 Interpretation

Fig. 13 gives an overview of the dispersion curves determined with the different methods. The curves are retrieved between 3 and 12 Hz with Rayleigh velocities ranging from about 1500 m/s at 3.5 Hz down to 600 m/s at 12 Hz for the fundamental mode. The results from WaveDec, though less smooth, agree with the 3C HRFK.

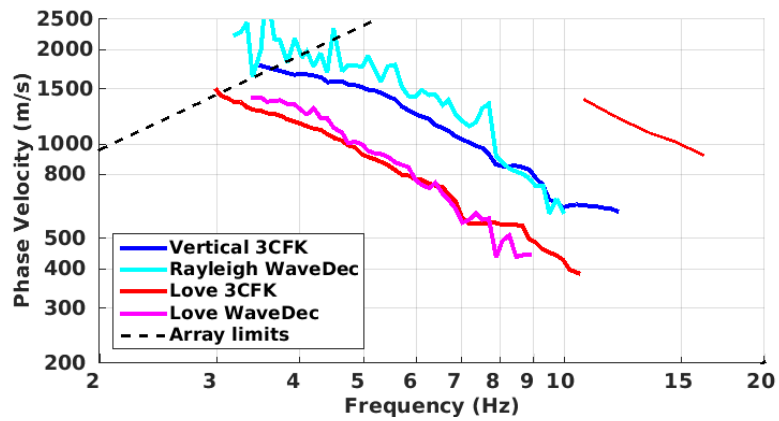


Figure 13: Picked dispersion curves from 3C HRFK analysis and the WaveDec method.

3.6 Data inversion

The inversion of the surface waves properties into 1D velocity profiles was performed using the Modified Neighborhood Algorithm (NA) (Wathelet, 2008) implemented in the Dinver software.

3.6.1 Misfit function

In the misfit function, the Rayleigh waves fundamental mode dispersion curve, the Love waves fundamental and first higher modes dispersion curves, the fundamental ellipticity peak at 4.5 Hz and the ellipticity curve around the 4.5 Hz peak (H/V curve from the TFA code of V. Poggi at APK000 point) and around the 7.6 Hz peak (WaveDec code) were used as simultaneous targets without standard deviation. A low weight of 0.05 was assigned to the ellipticity peak and to the ellipticity curve. All curves were resampled using 50 points between 2 and 20 Hz in log scale.

3.6.2 Parametrization of the model space

The velocity was assumed to increase with depth. No velocity inversion is needed to explain the observed data. The Poisson ratio was inverted in each layer in the range 0.2-0.4 (no aquifer). The density was assumed to be 2000 kg/m³ in the first layers and 2500 kg/m³ in the rock layers. Inversions with free layer depths as well as fixed layer depths were performed. 5 independent runs of 5 different parametrization schemes (5 and 6 layers over a half space and 10, 11 and 12 layers with fixed depth) were performed, i.e. a total of 25 runs.

3.6.3 Results

Examples of retrieved ground profiles for these two strategies are presented in Fig. 14. When comparing to the target curves (Fig. 15), dispersion curves are generally well reproduced as well as the shape of the ellipticity. For further elaborations, the best model of each 25 runs was selected and used (see section 4.1).

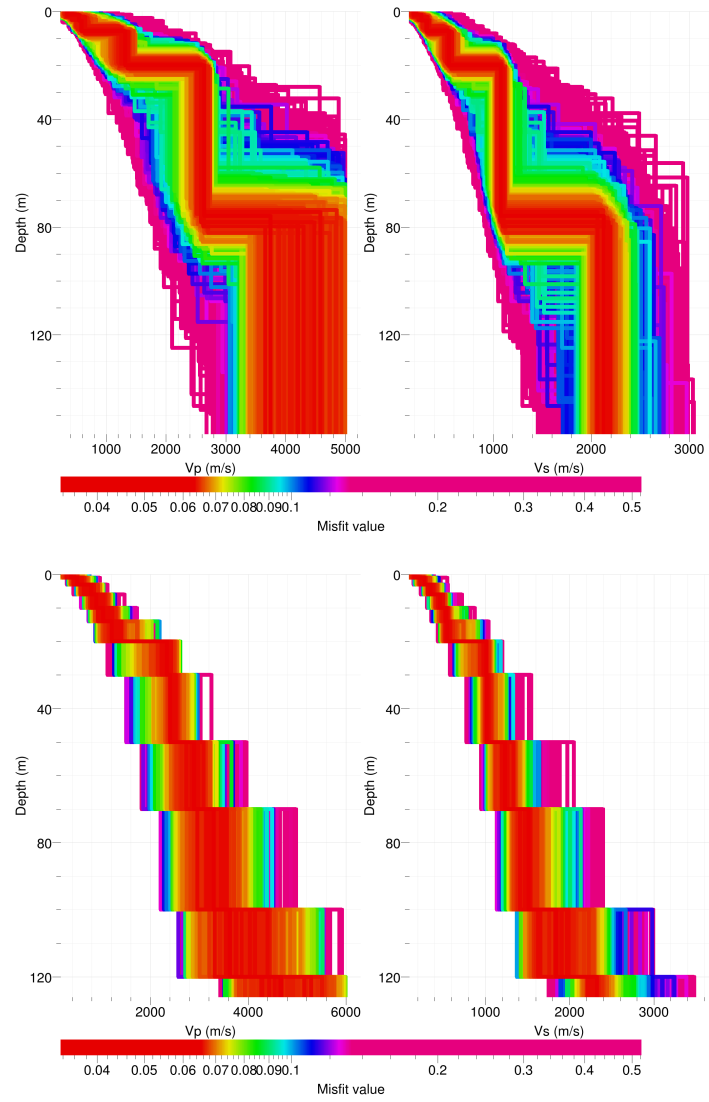


Figure 14: Inverted ground profiles at SAPK in terms of V_p and V_s ; top: free layer depth strategy; bottom: fixed layer depth strategy.

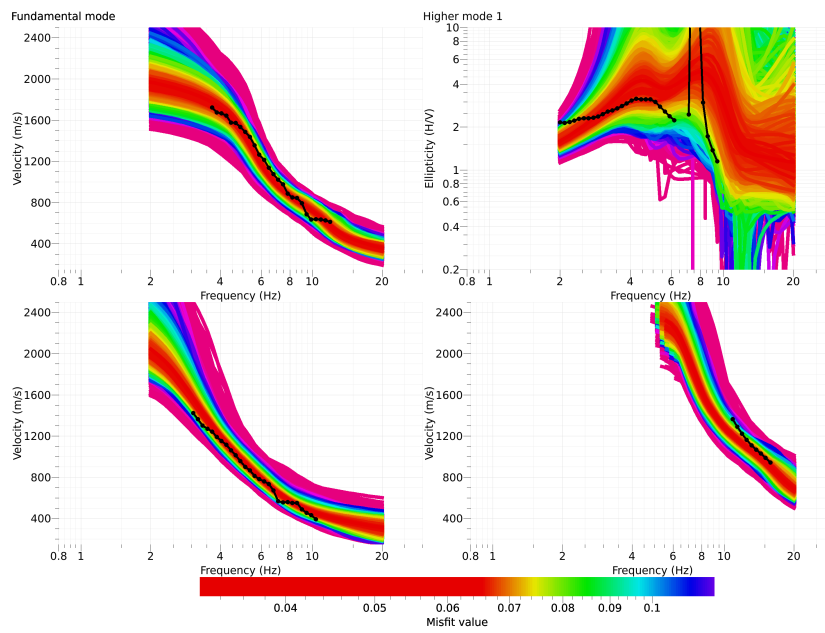


Figure 15: Comparison between inverted models and measured Rayleigh waves (top row fundamental mode: left, fundamental mode ellipticity: right) and Love waves (bottom row left: fundamental mode; right: first higher mode) properties at site SAPK for the fixed layer depth strategy.

4 Interpretation of the velocity profiles

4.1 Velocity profiles

The velocity (Fig. 16) is increasing in the first 5 meters of the profile from 200 to 400 m/s. Below, a homogeneous layer at about 500 m/s interpreted as moraine is found down to about 17 m depth (± 2 m). The available borehole, located close to APK401, compares well with this result: 26 m of moraine were found there for a resonance frequency that is lower (3.5 Hz) than in the array centre (4.5 Hz).

The velocity contrast is strong with the underlying rock (Lower Freshwater Molasse) at about 1000 m/s. The velocity increases below 80 m depth (the velocity jump in the free layer depth models is probably due to the limited number of allowed layers in the inversion) up to about 2000 m/s at 120 m depth but with a low constraint from the data.

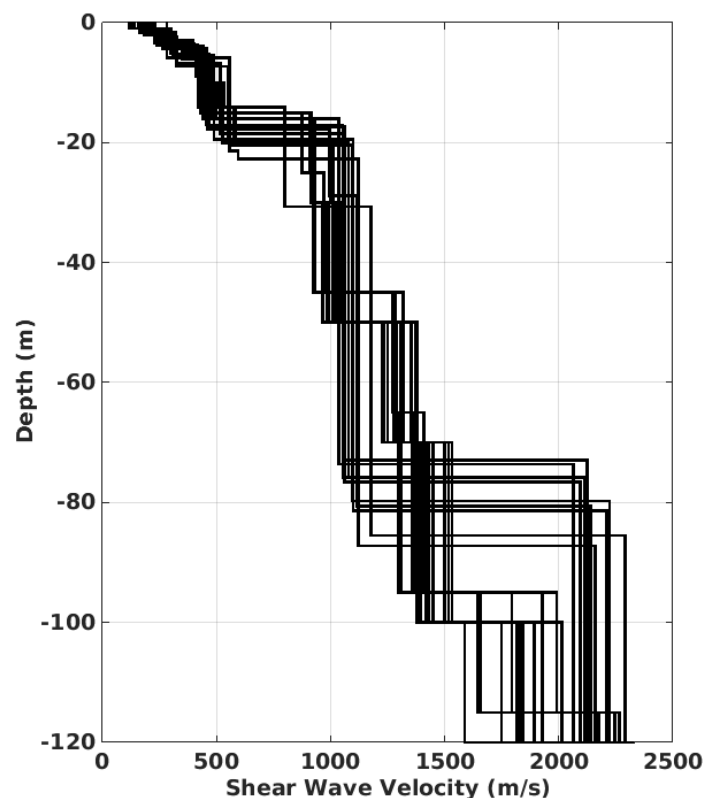


Figure 16: Shear-wave velocity profiles of the 25 selected models.

The distribution of the travel time average velocities at different depths was computed from the selected models. $V_{s,30}$ is found to be 509 m/s. The velocity profiles correspond to the definition of ground type E in the Eurocode 8 (CEN, 2004) and the SIA261 (SIA, 2014): less than 20 m of sediments of average velocity of 360 m/s (≤ 360 m/s required in the EC8, ≤ 500 m/s in the SIA261) over a bedrock of velocity 1000 m/s (≥ 800 m/s required). It is therefore at the border for the EC8 definition.

4.2 Quarter-wavelength representation

The quarter-wavelength velocity approach (Joyner et al., 1981) provides, for a given frequency, the average velocity at a depth corresponding to $1/4$ of the wavelength of interest. It is useful to identify the frequency limits of the experimental data (minimum frequency in dispersion curves at 3 Hz, in the ellipticity curve at 2 Hz). The results using this proxy show that the dispersion curves constrain the profiles down to 60 m and the ellipticity to about 110 m (Fig. 17). Furthermore, the dispersion data up to 15 Hz ensure reliable results below 4 m depth. Moreover, the quarter wavelength impedance-contrast introduced by Poggi et al. (2012a) is also displayed in the figure. It corresponds to the ratio between two quarter-wavelength average velocities, respectively from the top and the bottom part of the velocity profile, at a given frequency (Poggi et al., 2012a). It shows a trough (inverse shows a peak) at the resonance frequency.

4.3 SH transfer function

The theoretical SH-wave transfer function for vertical propagation (Roesset, 1970) is computed from the selected profiles. It is corrected with respect to the Swiss Reference Rock model (Poggi et al., 2011) following Edwards et al. (2013). It shows a small peak at the fundamental frequency of resonance (3.5 Hz) and a larger one at 7 Hz with an amplification of 2 and 3.5, respectively (Fig. 18). It is compared to the amplification function obtained by empirical spectral modelling (ESM) though few recordings are available to date (Edwards et al., 2013; Michel et al., 2014, 2016). The theoretical SH transfer function of the retrieved profiles matches well the observed amplification function at station SAPK (Fig. 18).

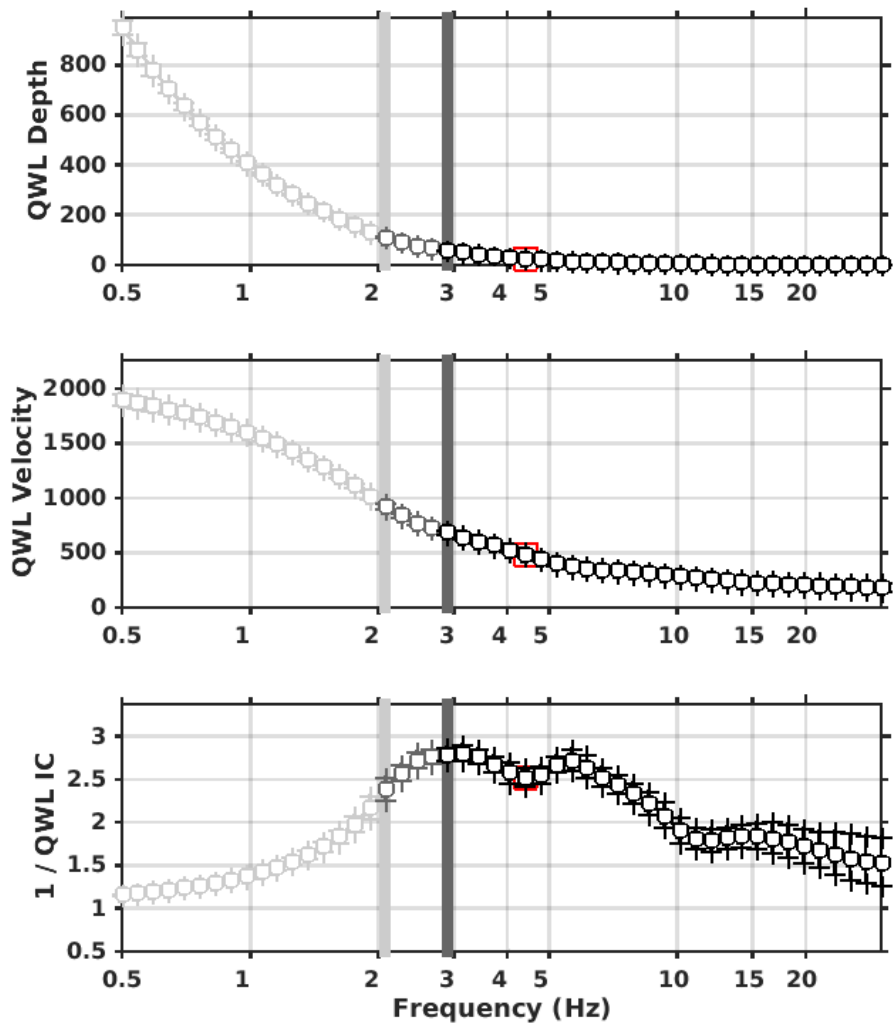


Figure 17: Quarter wavelength representation of the selected velocity profiles (top: depth, center: velocity, bottom: inverse of the impedance contrast). The black curves are constrained by the dispersion curves, the light grey curves are not constrained by the data. The red square corresponds to V_{S30} .

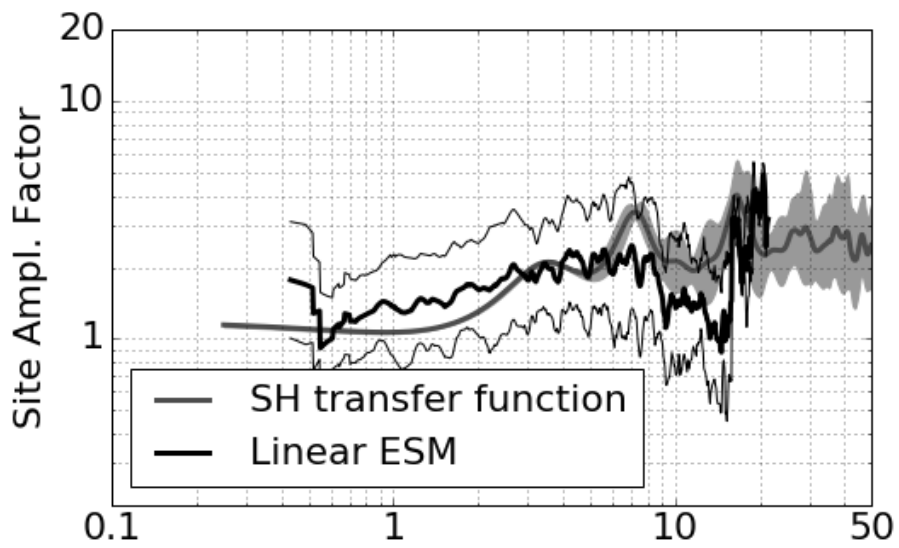


Figure 18: Comparison between the modeled SH transfer function for the selected velocity profiles and the empirical amplification (ESM) measured at station SAPK (with standard deviation).

5 Conclusions

The passive measurements presented in this study were successful in deriving a velocity model for the site SAPK. The soft sediment cover (moraine) is about 17 m thick with a low velocity over the 5 first meters and of about 500 m/s below. The rock located underneath (Lower Freshwater Molasse) has a velocity of about 1000 m/s. Another noticeable increase of velocity is found below 80 m depth. This report also presented an insight of the distribution of the sediment cover in the town.

$V_{s,30}$ is 509 m/s and the site corresponds to ground type E in the Eurocode 8 (CEN, 2004) and in the SIA261 (SIA, 2014). The theoretical 1D SH transfer function computed from the inverted profiles shows an amplification of a factor of 2 to 3 at the resonance frequencies of the velocity structure at 3.5 and 7 Hz.

Acknowledgements

The authors thank Simon Rouwendaal and David Farsky for their help with the array measurements and Raphaela Büsser from canton Appenzell Innerrhoden who looked for available boreholes.

References

- Baumann, C., Burjánek, J., Michel, C., Fäh, D., and Dalguer, L. a. (2013). Fault zone signatures from ambient vibration measurements: a case study in the region of Visp (Valais, Switzerland). *Swiss Journal of Geosciences*, 106(3):529–541.
- Burjánek, J., Gassner-Stamm, G., Poggi, V., Moore, J. R., and Fäh, D. (2010). Ambient vibration analysis of an unstable mountain slope. *Geophysical Journal International*, 180(2):820–828.
- CEN (2004). *Eurocode 8: Design of structures for earthquake resistance - Part 1: General rules, seismic actions and rules for buildings*. European Committee for Standardization, en 1998-1: edition.
- Edwards, B., Michel, C., Poggi, V., and Fäh, D. (2013). Determination of Site Amplification from Regional Seismicity : Application to the Swiss National Seismic Networks. *Seismological Research Letters*, 84(4).
- Fäh, D., Kind, F., and Giardini, D. (2001). A theoretical investigation of average H/V ratios. *Geophysical Journal International*, 145(2):535–549.
- Joyner, W. B., Warrick, R. E., and Fumal, T. E. (1981). The effect of Quaternary alluvium on strong ground motion in the Coyote Lake, California, earthquake of 1979. *Bulletin of the Seismological Society of America*, 71(4):1333–1349.
- Maranò, S., Reller, C., Loeliger, H. A., and Fäh, D. (2012). Seismic waves estimation and wavefield decomposition: Application to ambient vibrations. *Geophysical Journal International*, 191(1):175–188.

- Michel, C., Edwards, B., Poggi, V., Burjánek, J., Roten, D., Cauzzi, C., and Fäh, D. (2014). Assessment of Site Effects in Alpine Regions through Systematic Site Characterization of Seismic Stations. *Bulletin of the Seismological Society of America*, 104(6):2809–2826.
- Michel, C., Fäh, D., Edwards, B., and Cauzzi, C. (2016). Site amplification at the city scale in Basel (Switzerland) from geophysical site characterization and spectral modelling of recorded earthquakes. *Physics and Chemistry of the Earth, Parts A/B/C*.
- Poggi, V., Edwards, B., and Fäh, D. (2011). Derivation of a Reference Shear-Wave Velocity Model from Empirical Site Amplification. *Bulletin of the Seismological Society of America*, 101(1):258–274.
- Poggi, V., Edwards, B., and Fäh, D. (2012a). Characterizing the Vertical-to-Horizontal Ratio of Ground Motion at Soft-Sediment Sites. *Bulletin of the Seismological Society of America*, 102(6):2741–2756.
- Poggi, V. and Fäh, D. (2010). Estimating Rayleigh wave particle motion from three-component array analysis of ambient vibrations. *Geophysical Journal International*, 180(1):251–267.
- Poggi, V., Fäh, D., Burjánek, J., and Giardini, D. (2012b). The use of Rayleigh-wave ellipticity for site-specific hazard assessment and microzonation: application to the city of Lucerne, Switzerland. *Geophysical Journal International*, 188(3):1154–1172.
- Prieto, G., Parker, R., and Vernon III, F. (2009). A Fortran 90 library for multitaper spectrum analysis. *Computers & Geosciences*, 35(8):1701–1710.
- Roesset, J. (1970). Fundamentals of soil amplification. In Hansen, R. J., editor, *Seismic Design for Nuclear Power Plants*, pages 183–244. M.I.T. Press, Cambridge, Mass.
- SIA (2014). *SIA 261 Einwirkungen auf Tragwerke*. Société suisse des ingénieurs et des architectes, Zurich, Switzerland.
- Wathelet, M. (2008). An improved neighborhood algorithm: Parameter conditions and dynamic scaling. *Geophysical Research Letters*, 35(9):1–5.